J Therm Anal Calorim (2012) 108:235–241
DOI 10.1007/s10973-011-1504-y

Quantification methods of amorphous/crystalline fractions in high-energy ball milled pharmaceutical products

Giovanna Bruni · Vittorio Berbenni · Franco Sartor · Chiara Milanese · Alessandro Girella · Dionigio Franchi · Amedeo Marini

Received: 11 January 2011 / Accepted: 17 March 2011 / Published online: 9 April 2011

Abstract In this work, thermoanalytical, diffractometry, and microscopy measurements have been performed in order to characterize the effect of high energy milling on a drug active in the migraine prophylaxis and smoke cessation. We can assert that the mechanical treatment induces only a partial amorphisation of the solid phase, in particular it reduces the crystal order by producing lattice defects which propagate from the surface to the bulk crystal. For this reason, the DSC is able to detect the presence of ordered solid, while the powder X-ray diffractometry, because of its low penetration depth, does not reach the crystalline core of the particles.

Keywords Amorphous phase · Crystalline solids · DSC · Mechanical activation · Milling

Introduction

In the formulation of a solid dosage form, great importance is given to the factors that may affect the technological properties of the powders, the drug stability, and its bioavailability as well. The drugs are mostly synthesized in crystalline form but, sometimes, they are obtained in fully or partially amorphous phase [1–8]. Crystalline solids are characterized by long-range order while amorphous materials exhibit short-range order [8]. Generally, the crystalline drug is the preferred form due to its inherent higher physical and chemical stability with respect to the amorphous phase. However, it has to be noted that the customary processes in the pharmaceutical formulation (milling, granulating, freeze-drying, and compacting) all can promote undesired amorphisation in the crystalline drug [9–12]. On the other hand the amorphous state can also be considered an advantage as it improves the bioavailability of the product [13, 14]: in these instances it is convenient to purposely obtain the drug into its amorphous state. As a matter of fact the amorphous state has a higher energy with respect to the crystalline one and so lower activation energy is required for dissolution [14–16]. The most commonly adopted methods to obtain amorphous phases are: condensation from the vapor phase, undercooling of the melt, mechanical activation by high energy milling of a crystalline powder, freeze-drying and spray-drying [9–12, 17, 18].

The aim of this work was to evaluate the possibility to obtain a drug into the amorphous phase by high energy ball-milling. Also we were aimed to find a method to quantify the amorphous part of a drug that, in this work, is a glycine receptor antagonist [(4E)-7-chloro-4-(2-oxo-1-phenyl-3-pyrrolidinylidene)-1,2,3,4-tetrahydro-2-quinolinecarboxylic acid, as meglumine salt] studied for the migraine prophylaxis and smoke cessation [19, 20].

Experimental section

Materials and treatments

GW468816E (code name) has been supplied by Glaxo-SmithKline (Verona, Italy). The following samples were

G. Bruni (✉) · V. Berbenni · C. Milanese · A. Girella · A. Marini
C.S.G.I. – Department of Chemistry, Division of Physical Chemistry, University of Pavia, via Taramelli 16, 27100 Pavia, Italy
e-mail: giovanna.bruni@unipv.it

F. Sartor
Aptuit Srl, via Fleming 4, 37135 Verona, Italy

D. Franchi
GlaxoSmithKline SpA, via Fleming 2, 37135 Verona, Italy

used: as received sample; samples milled in an agate ball mill (Planetary Micro Mill Pulverisette P7, Fritsch) under different experimental conditions: 300 rpm for 1, 8 and 16 h 400 rpm for 36 h; glassy phase obtained after drug melting.

Apparatus and procedures

Micrographs were collected with a Cambridge Stereoscan 200 scanning electron microscopy (SEM) on gold-sputtered samples.

Differential scanning calorimetry (DSC) measurements were carried out with a DSC 2920 apparatus (TA Instruments, New Castle, DE) interfaced with a TA 5000 data station. Temperature and enthalpy calibrations were performed by running ultrapure (99.999%) indium samples (m.p. = 156.6 °C). Standard aluminum pans were used in open or sealed configuration. The heating rate (β) varied from 1 to 20 K/min for measurements with the as-received sample and was 10 K/min with ball-milled samples. The cell was flushed with dry nitrogen (3 L/h).

Differential scanning calorimetry (DSC) measurements with temperature modulation (TMDSC) were performed both in open and sealed pans at heating rate of 1 K/min with a modulation period (P) of 60 s and temperature amplitude (A_T) of 0.159 °C in order to keep a modulated heating rate oscillating between 0 K/min and 2 K/min.

Thermogravimetric (TG) measurements were carried out with a TGA 2950 apparatus (TA Instruments) interfaced with a TA 3100 data station. The heating rate varied from 1 to 20 K/min. The cell was flushed with dry nitrogen (3 L/h). In the TG measurements, the samples were placed directly in the open Pt-holder or in aluminum sealed pans put on the same Pt-holder.

Powder X-ray diffraction (XRD) patterns were recorded with a powder diffractometer Bruker D 5005 connected to a goniometer. CuKα radiation monochromatized by a bent graphite crystal was used. Patterns were collected in step scan mode (step: 0.020°, counting time: 3 s) in the angular range 6–35°2ϑ. The powder was manually pressed inside the standard grooved sample holder. All spectra were collected in air at room temperature.

Results and discussion

As-received sample

The powder of GW468816E consists of greenish-yellow particles in the form of smooth platelets with a maximum size of 300 μm (Fig. 1). The XRD patterns in Fig. 2 show sharp reflections characteristic of a crystalline structure. A DSC scan that is representative of GW468816E (open pan, 10 K/min) is reported in Fig. 3: a sharp peak is present due to melting (T_{onset} = 189 °C) that is followed by an endothermal drift of the baseline attributable to decomposition. The thermogravimetric analysis shows that with β = 10 K/min (open pan) the sample mass keeps constant up to 187 °C; at $T > 187$ °C the decomposition sets out at a temperature that increases with heating rate.

The quantitative data from DSC and TG measurements performed with different experimental configurations and at different scan rates are listed in Table 1.

It is evident that, when $\beta \geq 10$ K/min, the onset temperature of the melting peak is nearly constant (≅190 °C) and the enthalpy change (ΔH) too is well reproducible (112.9 ± 2.9 J/g). The last column of Table 1 reports the temperature where the sample decomposition becomes

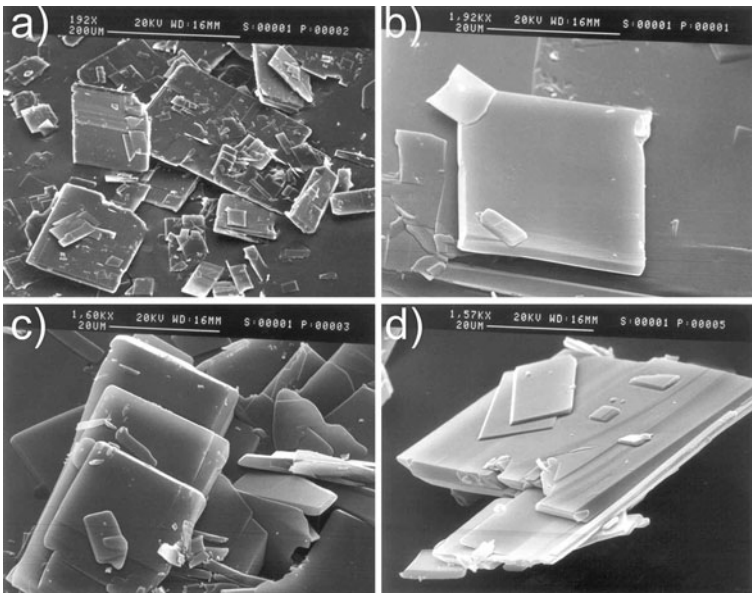

Fig. 1 SEM photographs of different particles of as-received GW468816E at different magnifications (**a**–**d**)

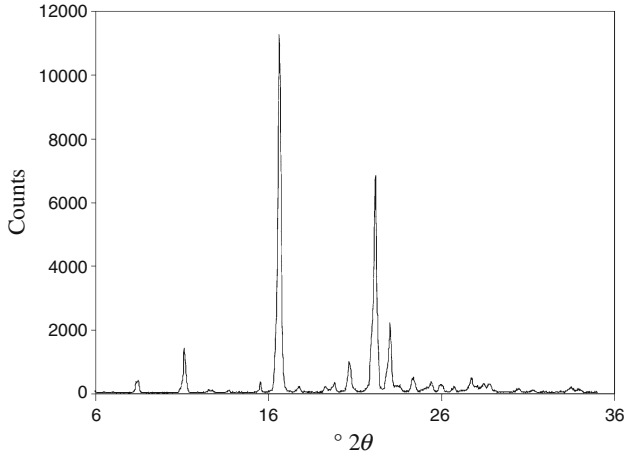

Fig. 2 XRD pattern of as-received GW468816E

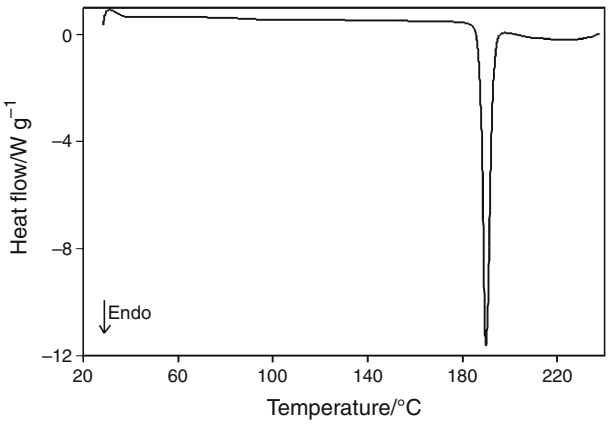

Fig. 3 DSC trace recorded on as-received GW468816E at 10 K/min in open pan

measurable from the TG curve (T_{dec}). At highest β, T_{dec} is close to the onset of melting indicating that melting occurs with decomposition. At lower β (2 K/min) the onset temperature of the DSC peak is 187 °C and the value of ΔH becomes significantly lower than that measured at high β. This result can be explained by noticing that T_{dec} is now lower than T_{onset} so that the contribution of the decomposition process is larger than it is at higher β. Clearly this results from the fact that the specific decomposition enthalpy is endothermic and moreover smaller than the melting enthalpy.

Ball-milled samples

1 h-long milling (300 rpm)

The effects of the milling on the morphology are evident in Fig. 4a–d. The mechanical treatment has destroyed the platelets present in the original powder considerably decreasing their size. Now the particles are micron-sized or submicron-sized, furthermore, they are also considerably

Table 1 Thermal parameters measured under different pan configurations and at different heating rate: onset temperature (T_{onset}) and enthalpy change (ΔH) of the melting peak and temperature of decomposition from TG measurements (T_{dec})

β/K min^{-1}	Pan configuration	T_{onset}/°C	ΔH/J g^{-1}	T_{dec}/°C
20	Open	191	111.0±2.5	192
20	Closed	190	114.6±0.6	
10	Open	189	110.1±2.9	188
10	Closed	189	114.4±1.9	
2	Open	187	100.7±1.5	181

aggregated. 1 h-long milling produces significant changes on the XRD pattern as well (Fig. 5, curve a). The reflections are present at the angular positions characteristic of the original sample (Fig. 2) but high energy milling seems to have affected the peak intensities that have become one order of magnitude lower and the relative intensities as well. We believe that these effects are due to the disappearance of preferred orientation present in the original sample. Furthermore, the reduction of the particle size (revealed by SEM) is reflected by the broadening of the peaks.

The thermal behavior of the 1 h-milled sample is slightly changed. Indeed both in open pan and sealed pan, the melting peak is present and its onset temperature and the relevant enthalpy change are only slightly decreased (at 10 K/min $T_{onset} = 187$ °C and $\Delta H = 104.6 \pm 4.5$ J/g).

8 h-long milling (300 rpm)

Scanning electron microscopy (SEM) pictures are shown in Fig. 6. 8 h-long milling caused the formation of acicular crystals. Micronic and submicronic particles with rounded edges cover their surface and are merged with it. In Fig. 5 (curve b), the dramatic change of the XRD pattern is evident. Though the SEM evidence shows a fair extent of crystallinity, the XRD reflections have almost disappeared and only a broad hump typical of an amorphous phase is present in the XRD patterns.

Some important results are shown by TG and DSC measurements. In the temperature range preceding the melting, some new effects are present as a consequence of the mechanical treatment that depends on the experimental configuration.

In open pan (Fig. 7) we observe:

– an initial endothermic hook of the DSC trace is associated to a non-reproducible mass loss (2–3.5%) which is over at about 75 °C,

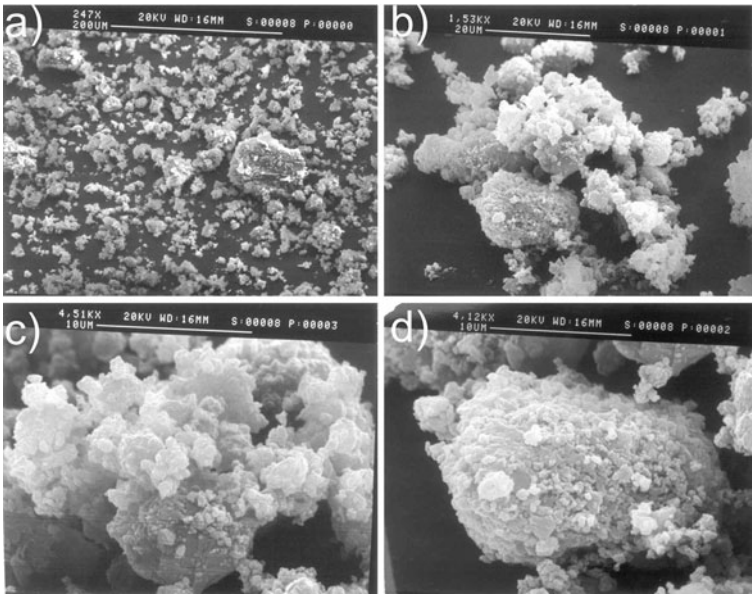

Fig. 4 SEM photographs of GW468816E 1 h milled (300 rpm) at different magnifications (**a**–**d**)

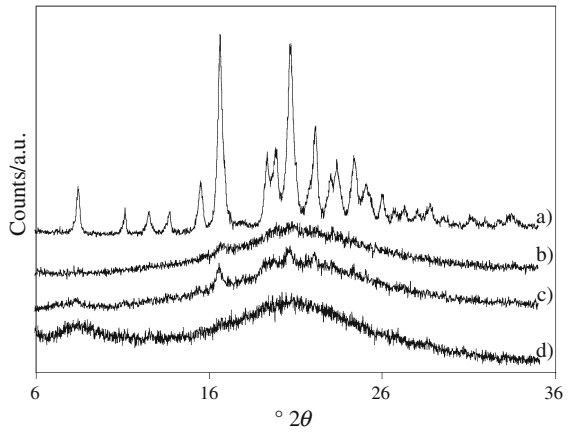

Fig. 5 XRD patterns of the ball-milled samples: 1 h (*a*), 8 h (*b*), 16 h (*c*), and 36 h (*d*)

- a glass transition at $T = 80$ °C with associated enthalpic relaxation,
- an exothermal peak ($T_{onset} = 106$ °C) with an enthalpy change of -32.7 ± 0.7 J/g.

We believe that the TG step (absent in the as received sample) is due to the release of water adsorbed on the sample surface due to milling. It is very likely that milling has produced a significant increase of the specific surface area of the sample, so it is not surprising the powder has adsorbed moisture.

The exothermal effect is reasonably due to the crystallization of the powder that has become amorphous as a consequence of ball-milling. Therefore, the enthalpy of the exothermic DSC peak shows that about 30% of the initial mass crystallizes during heating. Furthermore the melting peak ($T_{onset} = 185$ °C) has a ΔH value of 94.2 ± 0.5 J/g corresponding to the melting of 83% of the initial mass. From the DSC data thus we can argue that ball-milling caused the transformation of $\approx$50% of the original crystalline sample into amorphous phase that only partially crystallizes during heating. Such a result is in disagreement with the XRD evidence that shows that the sample has become, after having been milled, totally amorphous. As a matter of fact, the attribution of the exothermic peak to the re-crystallization process is confirmed by XRD results obtained on the samples heated up to different temperatures. Figure 8 shows the patterns of the 8 h-long milled sample: the (a) pattern pertains to the 8 h-milled sample as it is while pattern (b) pertains to the 8 h-milled sample put into an open pan and suddenly introduced into DSC cell that was kept at 85 °C which is the temperature just lower than the onset of the exothermal peak: both patterns are characteristic of a completely amorphous phase. Pattern (c) refers to a sample milled for 8 h, put into an open DSC pan and suddenly introduced into the DSC cell that was kept at 140 °C, i.e. at a temperature where the exothermic effect is just over. The pattern (c) shows diffraction effects that closely resemble those pattern reported in curve 5b (1 h-milled sample).

The TMDSC measurements confirm that the thermal event at 80 °C is due to a glass transition with enthalpic relaxation. In fact, as it is evident in Fig. 9, an endothermic peak is present in the non-reversing signal, while only a baseline shift shows in the reversing signal.

In closed pan (Fig. 10), the thermal behavior is more complicated

- both the glass transition ($T_{onset} = 45$ °C) and the exothermic peak ($T_{onset} = 74$ °C) appear at lower

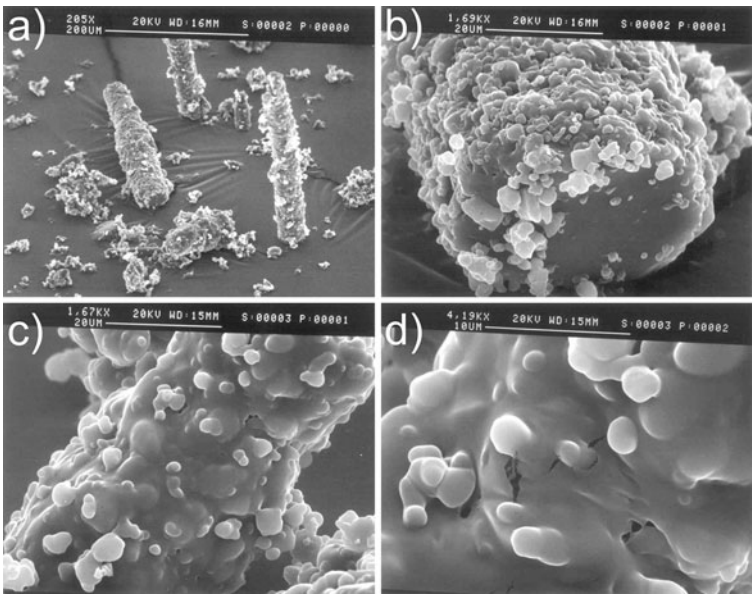

Fig. 6 SEM photographs of GW468816E 8 h milled (300 rpm) at different magnifications (**a**–**d**)

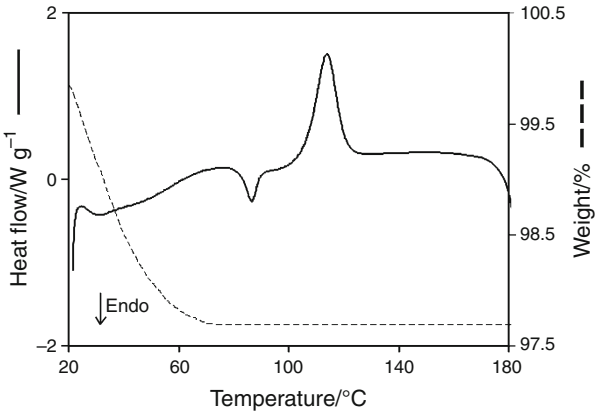

Fig. 7 DSC and TG traces recorded in open pan (10 K/min) with the 8 h-milled sample

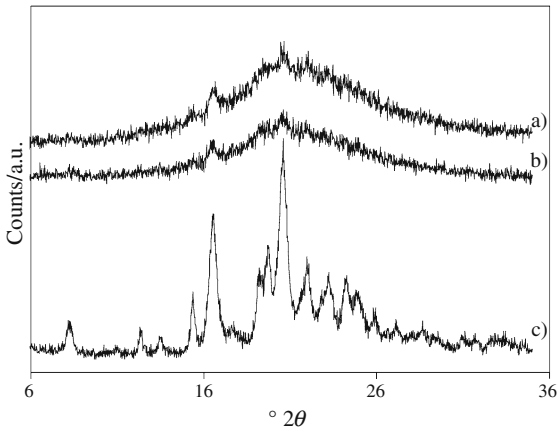

Fig. 8 XRD patterns of 8 h milled sample (*a*), brought to 85 °C (*b*) and to 140 °C (*c*)

temperatures. The heat released under the exothermic peak is -34.3 ± 1.7 J/g that is very close to the value obtained in the run performed in open pan (it corresponds to $\approx 30\%$ of the re-crystallization);

- the exothermic peak is followed by a new broad endothermic peak whose area is quite non reproducible ($T_{max} = 107$ °C, $\Delta H = 10 \div 25$ J/g). Such a peak is related to a variable mass loss;
- the melting peak is present at the same onset temperature as in open pan and yields the same enthalpy change.

The sealed pan effectively controls the water release so that it is shifted toward high temperature. This consideration allowed to explain the reason why the glass transition and, as a consequence, the exothermal peak are anticipated

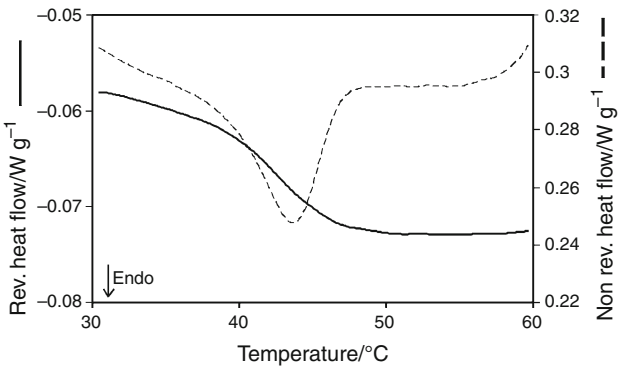

Fig. 9 TMDSC curves recorded in open pan (1 K/min) with the 8 h-milled sample

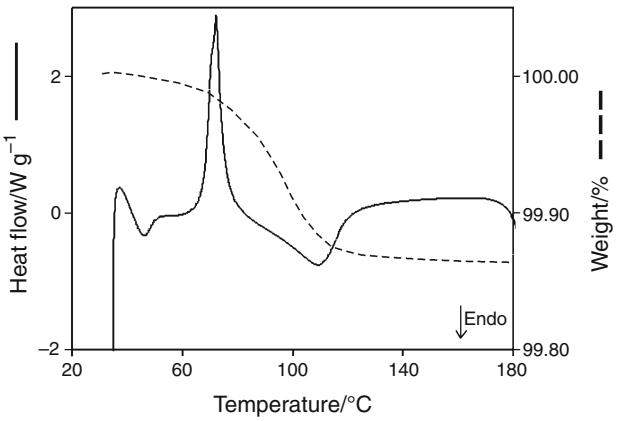

Fig. 10 DSC and TG traces recorded in closed pan (10 K/min) with the 8 h-milled sample

in closed pan: in this experimental configuration, water exerts a plasticizer effect and lowers the glass transition [21, 22]. The transition from glassy to rubbery state is necessary in order to reach enough molecular mobility for the crystallization to be triggered and this explains the fact that both glass transition and crystallization are anticipated when performing the DSC run in closed pan.

Also with this experimental configuration (closed pan), as expected, the thermal effects preceding the sample melting are not reversible.

16 h-long milling (300 rpm)

The sample morphology is shown in Fig. 11. The micron and submicron particles appear to be aggregated and it is evident that a "surface melting" occurred as a consequence of milling. The XRD pattern (Fig. 5 curve c) and the thermal behavior are roughly the same as those of the 8 h-long milled sample.

36 h-long milling (400 rpm)

The sample morphology and the XRD patterns (Fig. 5 curve d) are not so different from those of the 16 h-long milled sample. On the contrary, the DSC trace recorded in open pan is different in that the exothermal peak is shifted to $T_{onset} = 124$ °C and the relevant enthalpy change is higher (56.5 ± 2.0 J/g). The amount of sample recrystallized during the DSC scan is equal to about 50% of the initial mass. Again the melting enthalpy peak does not show differences with respect to the melting enthalpy values obtained for the samples milled for 8 and 16 h.

Melted sample

Cooling a melted sample yields an amorphous solid whose XRD pattern is shown in Fig. 12a. Such a solid, when crushed, shows upon re-heating (in open pan) a weak glass transition at 80 °C and an exothermic peak at $T_{onset} = 143$ °C followed by melting peak ($T_{onset} = 175$ °C). In this case, the enthalpies associated to the two peaks are nearly the same (≈55 J/g), suggesting that crystallization and melting occur to nearly the same extent. Now, however, just only about half of the initial mass of the sample melts. The partial crystallization of the melted sample during its heating is confirmed by XRD and SEM measurements. Indeed the pattern of a sample melted and heated up to 152 °C (when the exothermal effect is over) in the DSC cell (Fig. 2b) shows the diffraction effects typical of the original sample although their intensity is significantly lower. Furthermore, in SEM micrographs it is evident that platelets with smooth surface such as those present in the original sample have grown from the surface of the particles (Fig. 13).

Conclusions

While the XRD results show that milling leads to a fully amorphous state, DSC measurements indicate that the mechanical treatment promoted the transformation of about half of the initial mass to amorphous phase that is responsible of the glass transition and of the exothermic peak and that does not undergo melting.

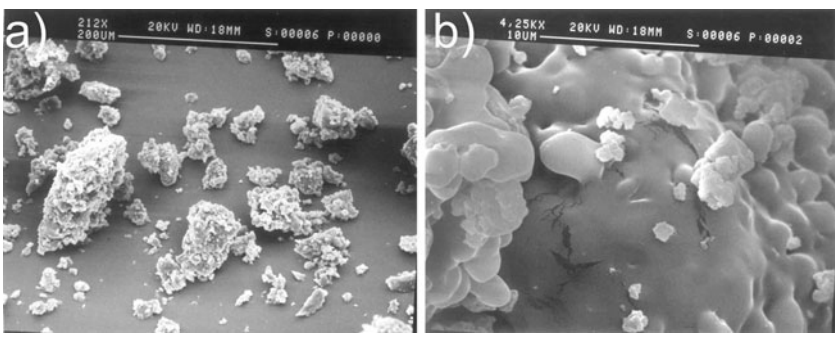

Fig. 11 SEM photographs of GW468816E 16 h milled (300 rpm) at different magnifications (**a**–**b**)

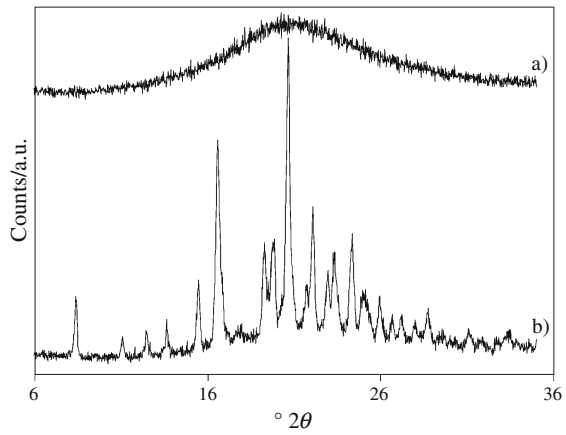

Fig. 12 XRD patterns of melted sample (*a*) and of melted sample heated up to 152 °C (*b*)

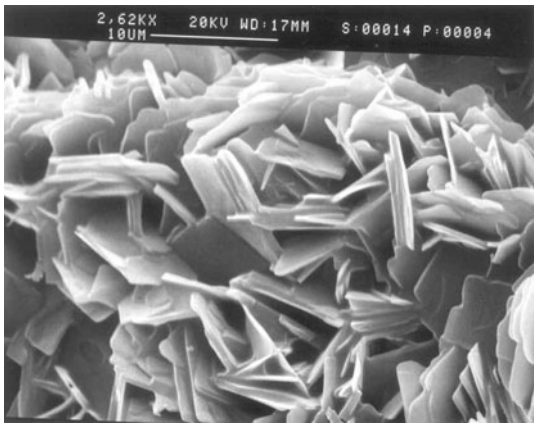

Fig. 13 SEM photograph of GW468816E melted and then heated up to 152 °C in the DSC cell

The apparent disagreement between the findings obtained by the two techniques may be explained as follows: as SEM pictures suggest, we can think that milling, besides reducing the particle size, causes the formation of an amorphous layer on the surface of the particles. This loss of crystalline order would be localized on the particles surface that is the only part of the sample "seen" by XRD due to their low penetration depth. The DSC response, on the contrary, originates from all the samples so that the DSC is able to identify and quantify the crystalline part of the sample. The results obtained by XRD and DSC perfectly agree when the sample to analyze is the melted one since, in this case, the amorphisation occurs throughout the whole sample.

Acknowledgements The authors would like to thank Dr. Sergio Bacchi of Aptuit Srl for helpful suggestion and discussion.

References

1. Vippagunta SR, Brittain HG, Grant DJW. Crystalline solids. Adv Drug Deliv Rev. 2001;48:3–26.
2. Hilfiker R, Blatter F, Raumer M. Relevance of solid-state properties for pharmaceutical products. In: Polymorphism in the pharmaceutical industry. Weinheim: Wiley-VCH; 2006. p. 1–19.
3. Marini A, Berbenni V, Bruni G, Cofrancesco P, Giordano F, Villa M. Physico-chemical characterization of drugs and drug forms in the solid state. Curr Med Chem. 2003;2:303–21.
4. Marini A, Berbenni V, Bruni G, Margheritis C, Orlandi A. Physicochemical study of the solid forms of a new drug. J Pharm Sci. 2001;90:2131–40.
5. Marini A, Berbenni V, Bruni G, Maggioni A, Cofrancesco P, Sinistri C, Orlandi A, Villa M. Solid state characterization of a novel chemotherapeutic drug. J Pharm Sci. 2003;92:577–84.
6. Bruni G, Berbenni V, Milanese C, Girella A, Cardini A, Viganò E, Lanfranconi S, Marini A. Thermodynamic relationship between nateglinide polymorphs. J Pharm Biomed Anal. 2009;50:764–70.
7. Bruni G, Milanese C, Bellazzi G, Berbenni V, Cofrancesco P, Marini A, Villa M. Quantification of drug amorphous fraction by DSC. J Therm Anal Calorim. 2007;89:761–6.
8. Yu L. Amorphous pharmaceutical solids: preparation, characterization and stabilization. Adv Drug Deliv Rev. 2001;48:27–42.
9. Willart JF, De Gusseme A, Hemon S, Odou G, Danede F, Descmps M. Direct crystal to glass transformation of trehalose induced by ball milling. Solid State Commun. 2001;119:501–5.
10. Brittain HG. Effects of mechanical processing on phase composition. J Pharm Sci. 2002;91:1573–80.
11. Elamin AA, Sebhatu T, Ahlneck C. The use of amorphous substances to study mechanically activated materials in the solid state. Int J Pharm. 1995;119:25–36.
12. Bruni G, Milanese C, Berbenni V, Sartor F, Villa M, Marini A. Crystalline and amorphous phases of a new drug. J Therm Anal Calorim. 2010;102:297–303.
13. Hutternrauch R. Modification of starting materials to improve tabletting properties. Pharm Ind. 1983;45:435–40.
14. Hancock B, Zografy G. Characteristics and significance of the amorphous state in pharmaceutical systems. J Pharm Sci. 1997;86:1–12.
15. Elamin AA, Ahlneck C, Alderborn G, Nystrom C. Increased metastable solubility of milled griseofulvin, depending on the formation of a disordered surface structure. Int J Pharm. 1994;111:159–70.
16. Hancock B, Parks M. What is the solubility advantage for amorphous pharmaceuticals. Pharm Res. 2000;17:397–404.
17. Vemuri NM, Chrzan Z, Cavatur R. Use of isothermal microcalorimetry in pharmaceutical preformulation studies Part II. Amorphous phase quantification in a predominantly crystalline phase. J Therm Anal Calorim. 2004;78:55–62.
18. Lappalainen M, Pitkanen I. Quantification of amorphous content in maltitol by StepScan DSC. J Therm Anal Calorim. 2006;84:345–53.
19. Charlton ST, Whetstone J, Fayinka ST, Read KD, Illum L, Davis SS. Evaluation of direct transport pathways of glycine receptor antagonists and an angiotensin antagonist from the nasal cavity to the central nervous system in the rat model. Pharm Res. 2008;25:1531–43.
20. Heidbreder C. Recent advances in the pharmacotherapeutic management of drug dependence and addiction. Curr Psychiatry Rev. 2005;1:45–67.
21. Kerč J, Srčič S. Thermal analysis of glassy pharmaceuticals. Thermochim Acta. 1995;248:81–95.
22. Alig I, Braun D, Langendorf R, Voigt M, Wendorff JH. Simultaneous ageing and crystallization process within the glassy state of a low molecular weight substance. J Non-Cryst Solids. 1997;221:261–4.